atmosphere

MDPI

Article

Evaluation of MERRA-2 Black Carbon Characteristics and Potential Sources over China

Mao Mao [1,*], Yu Zhou [2] and Xiaolin Zhang [2,3]

[1] Key Laboratory of Ecosystem Carbon Source and Sink, School of Atmosphere Science and Remote Sensing, Wuxi University, Wuxi 214105, China
[2] Key Laboratory for Aerosol-Cloud-Precipitation of China Meteorological Administration, School of Atmospheric Physics, Nanjing University of Information Science & Technology, Nanjing 210044, China
[3] State Key Laboratory of Atmospheric Boundary Layer Physics and Atmospheric Chemistry, Institute of Atmospheric Physics, Chinese Academy of Sciences, Beijing 100029, China
* Correspondence: mmao@nuist.edu.cn

Abstract: Black carbon (BC), an important component of atmospheric aerosol, plays a significant role in regional climate, hydrological cycle, variation of monsoon rainfall, and human health. The 40-year detailed atmospheric BC over China from 1981 to 2020 is systematically investigated through the MERRA-2 reanalysis dataset. MERRA-2 BC generally showed a good correlation (R = 0.68) compared with 673 monthly samples from ground-based observation at 35 stations around China. The overall annual average of MERRA-2 BC concentration over China is 1.15 μg/m^3, with a fast growth rate during 1981–2007 and a relatively slow decrease after that. The winter season has the highest mean concentration of BC, followed by autumn and spring, whereas summer shows relatively weaker values. The order of annual average BC concentrations during 1981–2020 is Beijing-Tianjin-Hebei region (BTH, 4.02 μg/m^3) > Sichuan Basin (SB, 3.94 μg/m^3) > Yangtze River Delta (YRD, 2.68 μg/m^3) > Pearl River Delta (PRD, 1.47 μg/m^3). The monthly mean BC concentrations over the BTH, YRD, PRD and SB are estimated to be smallest 3.18 μg/m^3 in May, 1.94 μg/m^3 in August, 0.82 μg/m^3 in July, 3.04 μg/m^3 in June, respectively, whilst largest consistently in December with 5.09 μg/m^3, 3.83 μg/m^3, 2.12 μg/m^3, and 5.41 μg/m^3, respectively. Our study indicates the primary potential source areas for BC are concentrated in the research city and its surroundings. Beijing and Chengdu are more BC-polluted areas than Shanghai and Guangzhou. Long-distance, regional transfer from south BTH contributes importantly to BC pollution in Beijing under the influence of prevailing southerly winds. The geographical location of Chengdu causes the transport and accumulation of BC inside the SB.

Keywords: black carbon; surface concentration; MERRA-2; potential source; China

Citation: Mao, M.; Zhou, Y.; Zhang, X. Evaluation of MERRA-2 Black Carbon Characteristics and Potential Sources over China. *Atmosphere* **2023**, *14*, 1378. https://doi.org/10.3390/atmos14091378

Academic Editor: Junwen Liu

Received: 11 July 2023
Revised: 15 August 2023
Accepted: 30 August 2023
Published: 31 August 2023

1. Introduction

Black carbon (BC) aerosols are mainly emitted as a primary pollutant of incomplete combustion of bio-fuel and fossil fuels, wildfires, and biomass burning [1,2]. BC strongly absorbs solar radiations, causing interference from atmospheric temperature gradients, and has become the No.2 factor in global warming, only behind CO_2 [3,4]. Freshly emitted BC particles are mostly bare monomers with chain-like structures, and they are quickly coated by secondary aerosol species during the aging process [5]. BC plays a significant role in regional climate, variation of monsoon rainfall, as well as the hydrological cycle over plateaus and mountain ranges [6–8]. Epidemiological studies revealed that BC pollution had adverse effects on human health [9–11]. More specifically, due to its fine particle size and porous structure, BC is able to carry toxic pollutants, such as heavy metals [12], polycyclic aromatic hydrocarbons, and volatile organic compounds, and readily penetrates into human lung tissue. Then, the uptake of these toxic chemical species by the alveolar epithelium enters the bloodstream [13]. In fact, cardiovascular diseases and carcinogenesis,

such as elevated systolic blood pressure, heart rate variability, and respiratory infections, have been confirmed to be partially associated with BC contamination [14–16]. The exposure to persistent BC tends to induce augmented premature mortalities and abated lung function [17–19].

Ground monitoring systems, numerical simulation, and satellite observation are the major approaches to investigating atmospheric BC aerosols. Nonetheless, stationary or mobile ground observation is unable to determine the region-scale pollution trends of BC by manual operation with relatively limited monitoring sites and small monitoring scope, while satellite remote sensing may miss, underestimate, or overestimate the data for certain days due to clouds and bright surfaces [20,21]. To compensate for the shortage of ground monitors and satellite data, a new innovation called 'data reanalysis' around the 1980s [22] was put forward by scientists, such as the National Centers for Environmental Prediction (NCEP) [23], Copernicus Atmosphere Monitoring Service (CAMS) [24], and version 2 of the Modern-Era Retrospective Analysis for Research and Applications (MERRA-2) [25,26]. These methods attempt to assimilate data from multiple sources and types with model simulations to achieve optimal integration. The MERRA-2 reanalysis data provide a good dataset with large spatial-temporal scales by remote sensing inversion technology to study the pollution characteristics of BC deeply since 1980.

In the last several decades, BC emissions in China have sharply increased, accounting for 25% of the global total emissions [1,27,28]. Research shows that the average life span of BC in the atmosphere environment is approximately seven days [29]. Accordingly, BC aerosol has enough time to take part in atmospheric physicochemical processes and reactions, as well as long-distance transport driven by air masses. With the continuous consumption of coal and fossil fuels, BC emission is an increasing threat to the environment, climate, and health and is urgent to be resolved. Since high BC concentration in China can be transported to other regions and countries under the influence of monsoon [30], it may have a certain impact on global BC concentrations, bringing enormous pressure to the government in environmental protection and climate negotiations. It is necessary to comprehensively allocate BC sources and subsequently implement effective mitigation measures, especially in areas with severe BC pollution. Although some studies regarding MERRA-2 BC concentration have been investigated [25,31–33], long-term and large-scale variation characteristics of detailed MERRA-2 BC concentration over China, especially in typical regions, are still scarce so far.

Here, spatial and temporal characteristics of atmospheric BC concentration over China during the period of 1981–2020 based on the MERRA-2 satellite reanalysis data are systematically carried out. The accuracy of MERRA-2 BC concentration with ground-based observations is also validated, and BC potential source region in typical cities based on the potential source contribution function (PSCF) and concentration weight trajectory (CWT) models is also evaluated. The paper is organized as follows. In Section 2, the data and method for BC concentration are introduced. In Section 3, the 40-year detailed characteristics of MERRA-2 BC concentration over China and its validation with ground observation and potential source region are discussed. The main conclusions are summarized in Section 4.

2. Data and Methodology

2.1. MERRA-2 Data

The MERRA-2 reanalysis dataset is produced by the Goddard Earth Observing System Model, Version 5 (GEOS-5) [34]. The MEERA-2 jointly assimilates meteorology and aerosol observations for aiming at integrated Earth system analyses, and it is the first time to include the aerosol fields radiatively coupled to the atmosphere [35]. At present, the MERRA-2 is the most significant long-term global reanalysis, representing the interactions of aerosols with other physical processes in the climate system [36]. A spatial resolution of $0.5^\circ \times 0.625^\circ$ and 72 vertical model levels from the surface to around 80 km are provided

in the MERRA-2 dataset, and it supplies 1-hourly, 3-hourly, and monthly products on the NASA website [37].

2.2. Ground Observation

This paper utilized the ground BC observation data obtained from literature published on the China Knowledge Network and Science Direct to verify the accuracy of MERRA-2 BC data in China (see Supporting Information). Related literature was collected, and the geographic coordinates (latitude and longitude) of the monitoring sites, as well as monthly BC concentration values, were extracted. More details about the observation station are presented in Table S1. Considering that one grid point of MERRA-2 BC data is sufficient to cover the observation site, the monthly mean data of MERRA-2 grid points close to the observation point is selected as the comparison value for observation. After statistical integration, we collected approximately 672 qualified monthly average BC concentrations from ground observation points and compared them with the corresponding grids in MERRA-2.

2.3. Methods

The PSCF, developed by Ashbaugh et al. [38], combines the results of 72-h air mass backward-trajectories (4 times per day, 0:00, 6:00, 12:00, and 18:00 UTC, the starting height of 500 m above the ground level, the meteorological database acquired from the Global Data Assimilation System [39]) for reflecting the proportion of polluted BC trajectories. The PSCF is expressed as:

$$PSCF_{ij} = \frac{m_{ij}}{n_{ij}} \tag{1}$$

where i and j denote the latitude and longitude, n_{ij} is on behalf of the total number of endpoints that fall in the ijth cell, and m_{ij} represents the number of endpoints in the same cell associated with samples for which the monitored mass concentration of pollutant exceeds a criterion BC value in the ijth cell. To eliminate the uncertainty in cells with a small value of n_{ij}, the PSCF values were multiplied by an arbitrary weighting function W (n_{ij}) [40,41], so the W (n_{ij}) can be described on Formula (2)

$$W(n_{ij}) = \begin{cases} 1.00, & 80 < n_{ij} \\ 0.70, & 20 < n_{ij} \leq 80 \\ 0.42, & 10 < n_{ij} \leq 20 \\ 0.05, & n_{ij} \leq 10 \end{cases} \tag{2}$$

Then, the weight WPSCF can be derived as follows:

$$WPSCF_{ij} = \frac{m_{ij}}{n_{ij}} \times W(n_{ij}) \tag{3}$$

The CWT model is applied to weight trajectories with related BC concentrations for identifying the relative contribution of different source areas [42]. Areas with high CWT values are considered as potential geographic origins of BC. The CWT is defined as follows:

$$C_{ij} = \frac{\sum_{h=1}^{M} C_h \times \tau_{ijh}}{\sum_{h=1}^{M} \tau_{ijh}} \times W(n_{ij}) \tag{4}$$

where C_{ij} represents the average weighted concentration in the ijth cell, h is the index of the trajectory, M is the total number of trajectories, C_h denotes the concentrations observed on arrival of trajectory h, τ_{ijh} is the time that trajectory h resides in the ijth cell. Similar to PSCF, the $W(n_{ij})$ is also utilized in the CWT method for reducing the uncertainty in cells:

$$WCWT_{ij} = C_{ij} \times W(n_{ij}) \tag{5}$$

Both PSCF and CWT analysis is run by the MeteoInfo soltware-TrajStat Plugin. More information about PSCF and CWT can be found elsewhere [40–47].

3. Results and Discussion

3.1. Validation of MERRA-2 BC Concentration with Ground-Based Observations

Figure 1 illustrates the comparison of monthly average BC surface concentration data at 35 stations (N = 672) between MERRA-2 products and ground observation in different regions of China. On the basis of the longitude and latitude of each station (Table S1), the proximate grid was picked out from MERRA-2, and the corresponding reanalysis values were adopted for validation. All correlation coefficients (R) for each site are significant at the level of 0.01. The R between MERRA-2 BC and ground observations was 0.68 (Figure S1), within diverse R values between 0.57 and 0.91 over six geographical regions.

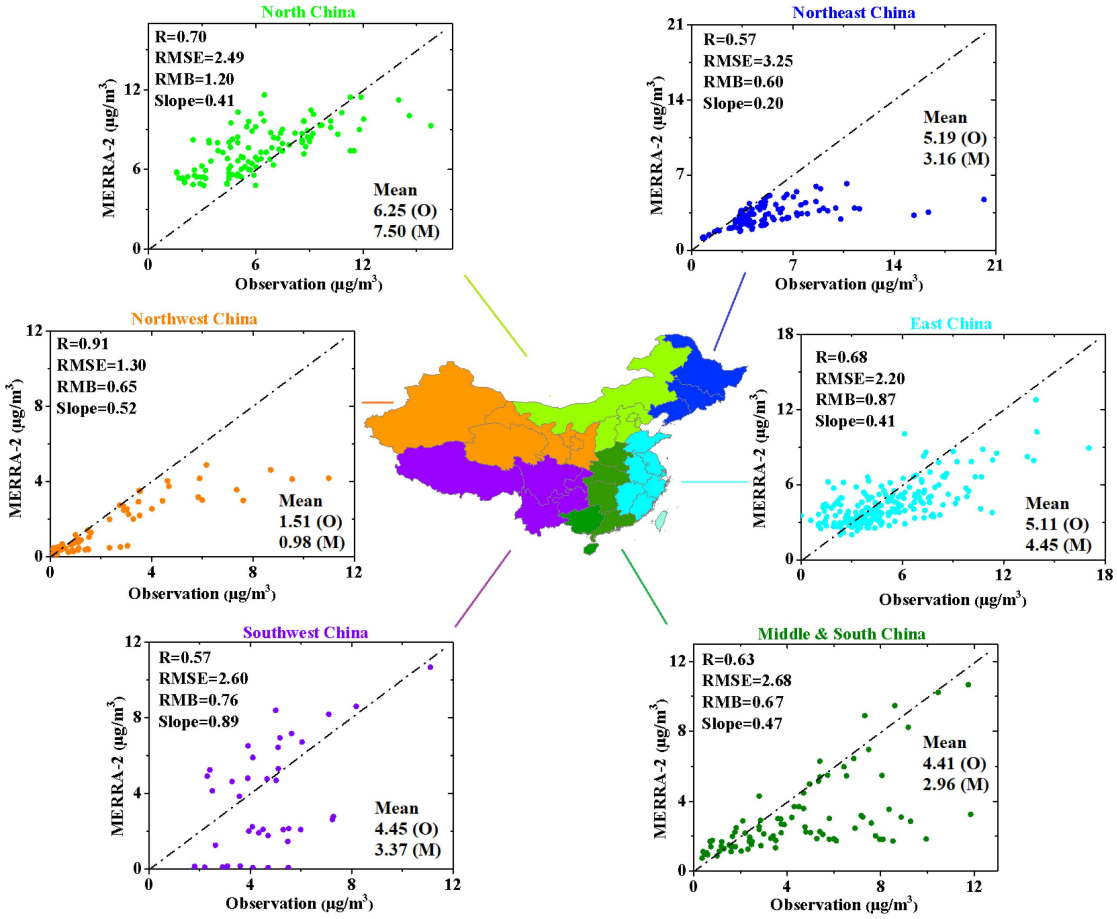

Figure 1. Comparison of the monthly average MERRA-2 BC concentration and ground observations. O and M represent the average BC concentrations of ground observation and MERRA-2.

The correlations in the Southwest and Northeast China (R = 0.57) were lowest, with 44 and 116 data, respectively, while the Northwest had the largest correlation (R = 0.91). The total slope was just 0.57, deviating from the predetermined 1:1 path (Figure S1), implying that MERRA-2 BC was smaller than the ground observation. Relative mean bias (RMB) and root mean square error (RMSE) are utilized to express the accuracy of MERRA-2 BC reanalysis data. MERRA BC data process credibility when RMB is over 0.5 [31]. The smaller the RMSE, the closer the MERRA-2 BC is to the ground observation. The reliabilities of MERRA-2 BC were all >0.5, with RMB in six regions between 0.61 and 1.20. Except that MERRA-2 overestimated BC concentration in North China (RMB = 1.20), MERRA-2 product underestimated BC concentration at most observations in Northeast (RMB = 0.61),

Northwest (RMB = 0.65), Middle and South (RMB = 0.63), and East China (RMB = 0.87). The scatter points in the Southwest were practically distributed on both sides of the middle 1:1 line. The smallest RMSE in Northwest (1.3 μg/m^3) makes for high credibility with six stations and one-hundred and eight samples. On the whole, the scatter plots portrayed a better correlation between MERRA-2 data and observation, and MERRA-2 BC was highly reliable around China (RMB = 0.85 > 0.5).

3.2. Spatial and Inter-Decade Variation of MERRA-2 BC Concentration

Figure 2 depicts the spatial distributions and inter-decade variations of MERRA-2 BC concentration over China for the years 1981–1990, 1991–2000, 2001–2010, and 2011–2020, respectively. In the past 40 years, the annual-averaged BC concentration in China is 1.15 ± 0.22 μg/m^3 and a growth rate of 1.30%. High BC concentrations generally occur in economically developed and densely populated Eastern-Central China. The vast but sparsely populated northwest region has a lower BC concentration below 0.5 μg/m^3.

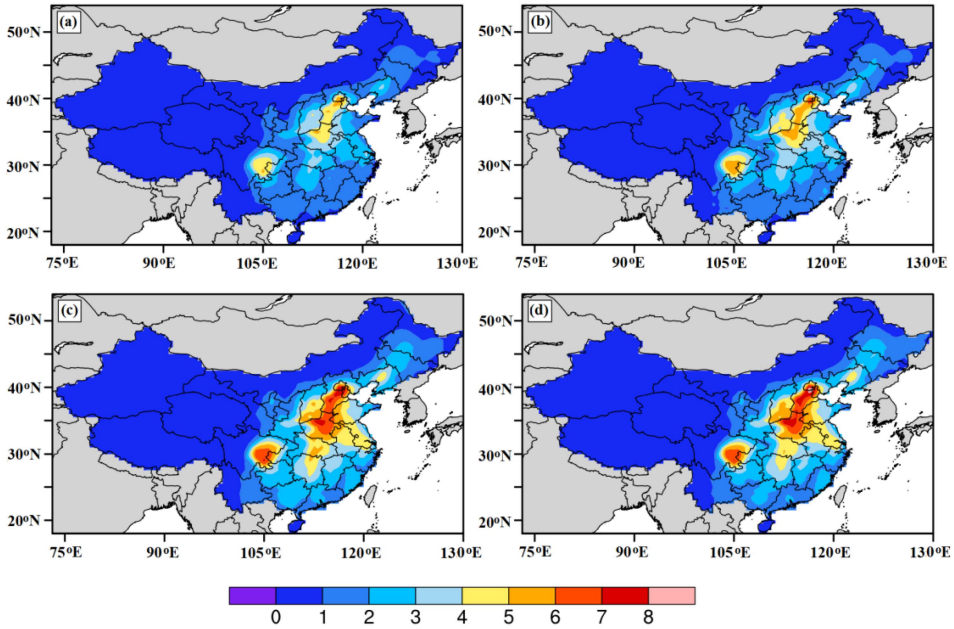

Figure 2. Spatial distributions of MERRA-2 BC concentration over mainland China for periods during the years of 1981–1990 (**a**), 1991–2000 (**b**), 2001–2010 (**c**), and 2011–2020 (**d**). Unit: μg/m^3.

As shown in Figure 2a, the BC concentration was relatively low during 1981–1990. Except for two BC high-value areas in the Sichuan Basin (SB), Beijing-Tianjin-Hebei region (BTH), and the neighboring Norther Henan, the BC concentration was below 4.0 μg/m^3 in most of China. The concentration in the above-mentioned areas has increased to 5.0 μg/m^3 during 1991–2000 (Figure 2b). With unprecedented levels of economic growth, the development of large-scale industries and services, the boom of vehicular population, and dramatic increases in energy consumption, the BC concentration on the ground is rapidly increasing. As displayed in Figure 2c, the values in SB, BTH, and the central and northern areas of Henan all exceeded 6.0 μg/m^3. Moreover, centered around the two BC high-value areas in Figure 2a, the BC high-value areas expanded outward during 2001–2010. BC pollution situation was also grim in the southern part of Shanxi and Henan provinces, the central part of Hunan province, the western part of Shandong province, the northern part of Anhui province, the vast majority of Jiangsu province, and some parts of Hubei province under the control of 4.00–6.00 μg/m^3. Especially for the central region of Hubei province, the highest BC concentration was found in four decades. The BC concentration in most of the central and eastern regions of China remained between 4.00 and 8.00 μg/m^3 during 2011–2020 (Figure 2d).

SB, BTH, and northern Henan have higher BC values, which may be attributable to some specific feature of local and regional emission sources mixed with meteorology influence. BTH is located in the eastern plains of China. Due to busy industries, strong human activities, and traffic congestion, the SB, BTH, and surrounding regions generate a large amount of BC emission and result in BC accumulation. Meanwhile, the coal consumption in BTH might be lower currently than decades ago due to the use of new technologies, but industrial and domestic heating is still an important source of coal-fired consumption and biomass burning, especially in North China. The transportation of air masses can also lead to changes in BC concentration. Sandstorms originating from the Northwest have a certain impact on the BTH region. The dusty and dry weather is not conducive to wet deposition. Additionally, the complexity of aerosol types is upgraded with the effect of warm and humid airstream in the Bohai Rim region.

Terrain is also an important factor affecting the spatial distribution of BC concentration. The SB region is surrounded by the Qinghai-Tibet Plateau, the Yunnan-Guizhou Plateau, Qinling-Daba Mountains. A relatively low-elevation basin surrounded by towering mountains and plateaus is more likely to have unique meteorological conditions such as high humidity and light wind [48]; thus, the diffusion of BC becomes difficult under the above conditions. The terrain in the Beijing Tianjin Hebei region exhibits a trend of high in the northwest and low in the southeast. When southerly winds prevail, it also promotes the accumulation of BC.

In brief, the high-value centers of MERRA-2 BC ground mass concentration are predominantly scattered over low-altitude basins and plains, e.g., the SB, BTH, and the surrounding northern part of Henan province.

3.3. Annual, Monthly, and Seasonal Variations of MERRA-2 BC Concentration over China

The annual analysis provides an overview of the BC concentration over China. As shown in Figure 3, the highest annual-averaged BC concentration was observed to be 1.48 $\mu g/m^3$ in 2007, and the lowest value was 0.74 $\mu g/m^3$ in 1981. In the early stage, the BC concentration was on a slow upward trend during 1981–1999 with an annual-averaged growth rate of 1.32% until it went straight to 0.99 $\mu g/m^3$ in 1999. The value began to rapidly increase from the year 2000 and reached the maximum in 2007 (a growth of 4.40% during 2000–2007), and then slowly decreased. The phenomenon may be mainly related to human activities. Along with rapid industrial development and urbanization, China has witnessed a fast-growing economy as well as increasing energy consumption, such as coal and oil, during the past two decades. Subsequently, as a coping mechanism against air pollution hazards and to protect public health, the Chinese government and local departments have taken various environmental measures to prevent and control air pollution. For example, in 2012, the Ministry of Environmental Protection (MEP) of China and the General Administration of Quality Supervision, Inspection and Quarantine jointly issued the Air Quality Standards (GB 3095-2012) [49]. Subsequently, MEP announced the 'Action Plan for Clean and Efficient Utilization of Coal 2015–2020' to reduce coal consumption in the year 2015. The BC concentration fluctuated significantly as a downward trend but remained at a high level during 2008–2020, indicating that more BC abatement policies need to be implemented over the long term.

The monthly and seasonal distributions (spring: MAM, summer: JJA, fall: SON, winter: DJF) using the whisker-box plots, which graphically depict numerical data via quartiles, are shown in Figure 4. Many factors, such as local emission, dry/wet deposition, and regional long-range transport, all play an important role in the temporal variation. The BC concentrations show a U-shaped trend. The valley appears in July (0.89 ± 0.15 $\mu g/m^3$) and reaches the peak in January (1.49 ± 0.34 $\mu g/m^3$) or December (1.50 ± 0.32 $\mu g/m^3$). The maximum value is almost two times greater than the minimum value. The seasonal average of BC concentrations over China are winter (1.42 ± 0.30 $\mu g/m^3$) > autumn (1.20 ± 0.24 $\mu g/m^3$) > spring (1.06 ± 0.21 $\mu g/m^3$) > summer (0.91 ± 0.15 $\mu g/m^3$), basically being in accordance with other research results in Yangtze River Delta (YRD) and BTH [50,51].

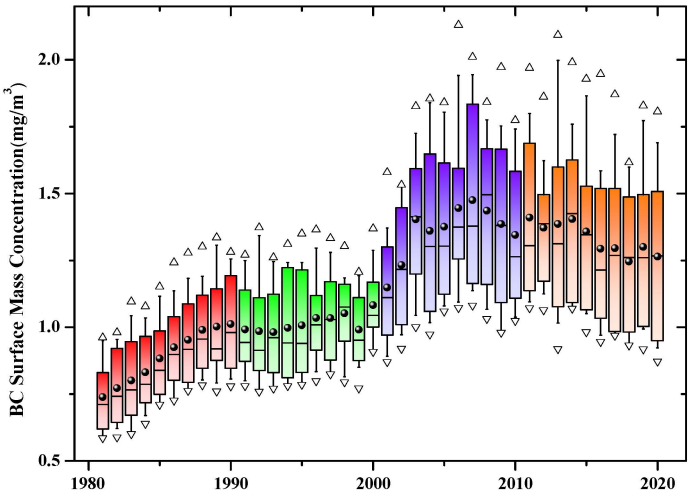

Figure 3. Annual variation trend of MERRA-2 BC concentration from 1981 to 2020 in China. The top and bottom whiskers show the 90th and 10th percentile, while the upper and lower boundaries of the central box show the 75th and 25th percentile. The middle line of the box represents the median, the solid circle represents the arithmetic average, and the positive triangle and inverted triangle represent max and min values, respectively. Red, green, purple, and orange represent the period of 1981–1990, 1991–2000, 2001–2010, and 2011–2020, respectively.

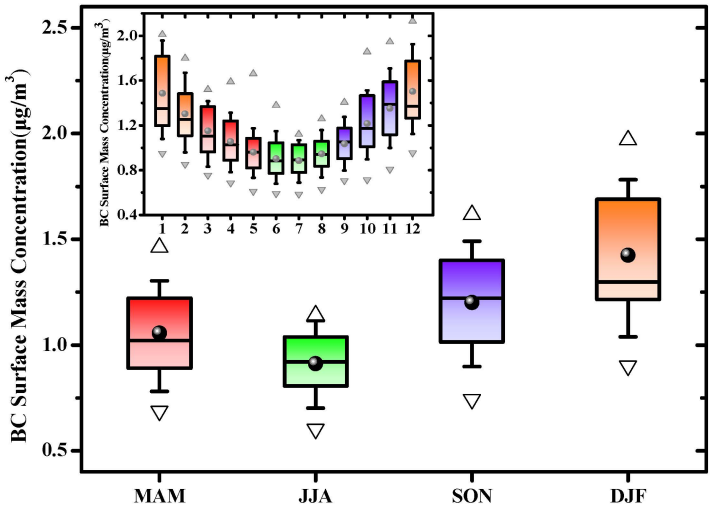

Figure 4. Seasonal and monthly variations of MERRA-2 BC concentration during 1981–2020 over China (MAM, JJA, SON, and DJF indicate spring, summer, fall, and winter, respectively). The top and bottom whiskers show the 90th and 10th percentile, while the upper and lower boundaries of the central box show the 75th and 25th percentile. The middle line of the box represents the median, the solid circle represents the arithmetic average, and the positive triangle and inverted triangle represent max and min values, respectively.

From Figure 4, it can be seen that there are a few large values in winter, as the average and median values are below the middle position between maximum and minimum, which could result from lasting stagnant weather with calm wind, low temperature, and less precipitation during the cold season [52]. The BC in areas with a well-economically developed and dense population contributes significantly to the overall BC concentration in China. The increasing energy consumption (e.g., coal and other fuels) for heating in winter, accompanied by the frequent occurrence of atmospheric inversion and lower boundary layer height, leads to the unfavorable dilution diffusion of BC, thus exacerbating pollution [53]. Additionally, residential heating emissions are close to the ground level and are likely to be higher per unit mass of coal than for boilers used in industrial heating

in cold weather. BC pollution from neighboring provinces using domestic and industrial heating should not be ignored. As for autumn, the frequent occurrence of agricultural open biomass burning activities, such as straw burning after harvest time, has elevated the BC level [54,55]. The BC concentrations in summer are the lowest among the four seasons. The more active atmospheric disturbance and higher boundary layer height associated with more frequent wet precipitation, such as rain scavenge caused by clean air flow from a maritime airstream or low latitudes, are advantageous to BC dilution, thus forming a relatively clean atmosphere environment status in hot summer.

3.4. MERRA-2 BC Concentration over Typical Areas of China

To better understand the spatiotemporal variations of BC concentrations in China, further comparisons in year-scale are analyzed in four typical geographic areas, including the BTH (region: 38–41° N, 114–119° E), YRD (region: 29–33° N, 117–122° E), Pearl River Delta (PRD, region: 22–24° N, 112–115° E), and SB (region: 28–32° N, 103–108° E) (Figure 5). In general, the annual average BC concentration during 1981–2020 followed the order of BTH (4.02 μg/m^3) > SB (3.94 μg/m^3) > YRD (2.68 μg/m^3) > PRD (1.47 μg/m^3). The yearly mean BC concentration during the decade of 1981–1990 (1.11–3.20 μg/m^3) and 1991–2000 (1.24–3.59 μg/m^3) was remarkably smaller than that during 2001–2010 (1.86–4.63 μg/m^3) and 2011–2020 (1.68–4.71 μg/m^3) in all four regions. In the PRD region, the yearly mean BC concentrations in PRD region varied from the smallest 0.93 μg/m^3 in 1981 to the largest value of 2.11 μg/m^3 in 2004. Nonetheless, the yearly average mean BC concentration in the BTH, YRD, and SB regions showed the smallest values of 2.48 μg/m^3 in 1981, 1.65 μg/m^3 in 1982, 2.67 μg/m^3 in 1981, respectively, whilst they had the largest 5.06 μg/m^3 in 2006, 3.56 μg/m^3 and 4.83 μg/m^3 in 2007, respectively.

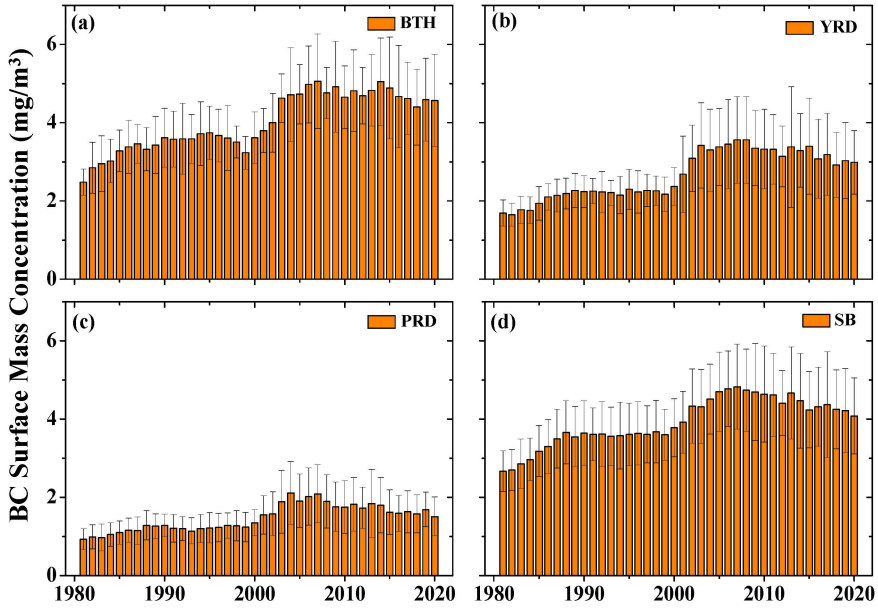

Figure 5. Annual variations of MERRA-2 BC concentration over the Beijing-Tianjin-Hebei region (**a**), Yangtze River Delta (**b**), Pearl River Delta (**c**), and Sichuan Basin (**d**) of China from 1981 to 2020. The error bar represents the standard deviation.

Four decades with the years 1981–1990, 1991–2000, 2001–2010, 2011–2020, and 1981–2020 are shown from top to bottom, while the seasonal and monthly averaged BC concentration over four typical regions of China are illustrated from left to right in Figure 6. In BTH, the highest concentration occurs in winter (4.83 μg/m^3), and the magnitude is very similar in summer and spring, with a value of 3.43 μg/m^3. Seasonal average BC concentrations in YRD also peak in winter (3.53 μg/m^3), followed by autumn (2.68 μg/m^3), spring (2.48 μg/m^3), and summer (2.01 μg/m^3); for the PRD region, 1.44, 0.89, 1.59, and

2.00 μg/m^3 are observed in spring, summer, autumn, and winter, respectively. Average BC concentrations in PRD in all seasons are similar, and the variance of BC is relatively low compared to BTH, PRD, and SB regions, indicating less anthropogenic BC aerosol emissions. In SB, average BC concentrations alleviate to some extent in summer (3.15 μg/m^3) compared to average concentrations in other seasons (about 3.48 μg/m^3 in spring, 4.14 μg/m^3 in autumn and 5.02 μg/m^3 in winter). The highest seasonal mean BC concentrations are observed in winter, whereas the lowest seasonal mean values are seen in summer for all four regions without exception. The seasonal variation pattern of BC concentration has not changed over recent decades, although strong seasonal averages are observed during 2001–2010 (Figure 6c) and 2011–2020 (Figure 6d), and weak values during 1981–1990 (Figure 6a) are seen.

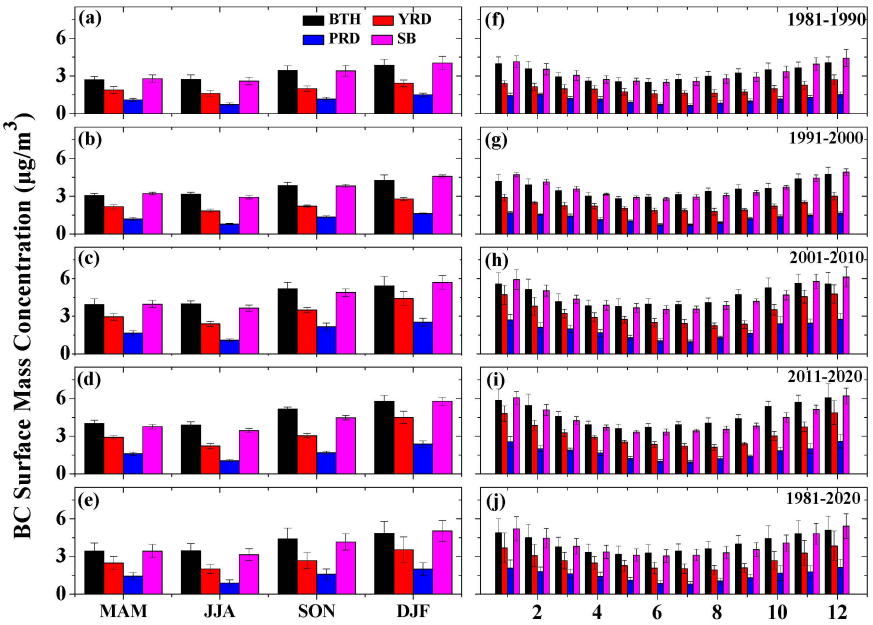

Figure 6. Seasonal and monthly average BC concentration in the BTH, YRD, PRD, and SB. The results for periods 1981–1990 (**a**,**f**), 1991–2000 (**b**,**g**), 2001–2010 (**c**,**h**), 2011–2020 (**d**,**i**) and 1981–2020 (**e**,**j**) are considered. Note: MAM (March, April, and May), JJA (June, July, and August), SON (September, October, and November), DJF (December, January, and February). The error bar represents the standard deviation.

Further analysis found that the monthly-averaged BC concentration in China during 1981–1990 (Figure 6f) and 1990–2000 (Figure 6g) was much smaller than that during 2001–2010 (Figure 6h) and 2011–2020 (Figure 6i). The monthly patterns of BC characteristics over four regions exhibit an almost identical trend and fluctuation consistent with their seasonal patterns. The monthly statistics illustrate that the monthly mean of PRD is considerably lower than that of the other three regions. The monthly average BC concentrations in BTH, YRD, PRD, and SB regions portray the smallest 3.18 μg/m^3 in May, 1.94 μg/m^3 in August, 0.82 μg/m^3 in July, 3.04 μg/m^3 in June, respectively. Under the domination of abundant rainfall with clean air low guided by East-Asia monsoons, aerosol can be effectively removed by wet precipitation. In summer months, trees thrive and flourish, as leaves have the most effective ability to capture BC from the ambient atmosphere. Strengthening city-virescence becomes one of the fundamental measures for weakening BC pollution to achieve the goal of purifying air in urban. In October, the elevated BC level may be caused by the agricultural open biomass burning activities after the harvesting of crops. From late autumn to severe winter months, most leaves wither and fall, reducing their water content to resist the approaching cold. Subsequently, the ability of trees to purify air decreases. The peak events of BC occur consistently in December, and the average BC concentrations for BHT, YRD, PRD, and SB are 5.09 μg/m^3, 3.83 μg/m^3, 2.12 μg/m^3, and 5.41 μg/m^3, respec-

tively. High alert levels of BC concentration are preserved between December and January, February, and March in the next year. The meteorological conditions in winter months and more energy combustion contribute to the formation of high BC pollution. In April, the BC concentrations reduced outstandingly, with corresponding values of 3.33 μg/m^3 in BTH, 2.49 μg/m^3 in YRD, 1.41 μg/m^3 in PRD, and 3.36 μg/m^3 in SB. The cessation of heating alleviates anthropogenic emissions. Meanwhile, as the weather warms, deciduous trees begin to sprout after dormancy, enhancing their ability to capture dust.

3.5. Pollutants Source Analysis Based on PSCF and CWT

The PSCF and CWT analyses are conducted to identify potential sources and the distribution of BC concentration contribution to the receptor sites. The PSCF model combines the results of a 72-h backward trajectory to reflect the proportion of polluted trajectories in a cell grid. The CWT model is applied to weight trajectories with related BC concentrations for identifying the relative contribution of different source areas. PSCF and CWT models complement each other, and areas with high PSCF/CWT values are supposed to be potential geographic origins of BC. Beijing, Shanghai, and Guangzhou are first-tier cities in eastern China and are municipalities directly under the central government. Chengdu is a representative city in central China. We chose Beijing, Shanghai, Guangzhou, and Chengdu as typical cities in BTH, YRD, PRD, and SB to analyze the potential source areas of BC.

The capital, Beijing, is located at the northern end of the BTH; some regions in the southeast are connected to Tianjin, with the rest being surrounded by Hebei province. Figure 7 reveals that in the four seasons of 2020, both high PSCF and CWT values with large amounts of BC for Beijing are seen in the BTH region. In spring, the southern region of Langfang, Baoding, and Tianjin had large contributions (PSCF > 0.7, CWT > 6 μg/m^3) to BC, as well as the southwestern directions, including Shijiazhuang, Cangzhou, Hengshui, Xingtai, and Handan in Hebei province, Anyang and Hebi in Heinan province with high contribution exceeding 0.6 for PSCF and 5 μg/m^3 for CWT. The average BC mass concentration in summer (6.78 μg/m^3) was larger compared to that of spring (6.08 μg/m^3) for Beijing in 2020. As a result, the potential source area of BC had a slightly wider distribution in summer, with the air mass traveling through Hebei, Tianjin, Shandong, and Northern Henan (PSCF > 0.4, CWT > 4 μg/m^3), reflecting a large scale and long-distance transfer of BC. Under the control of the prevailing southeast monsoon, the rapidly moving air masses in summer contributed to the BC dilution in Beijing.

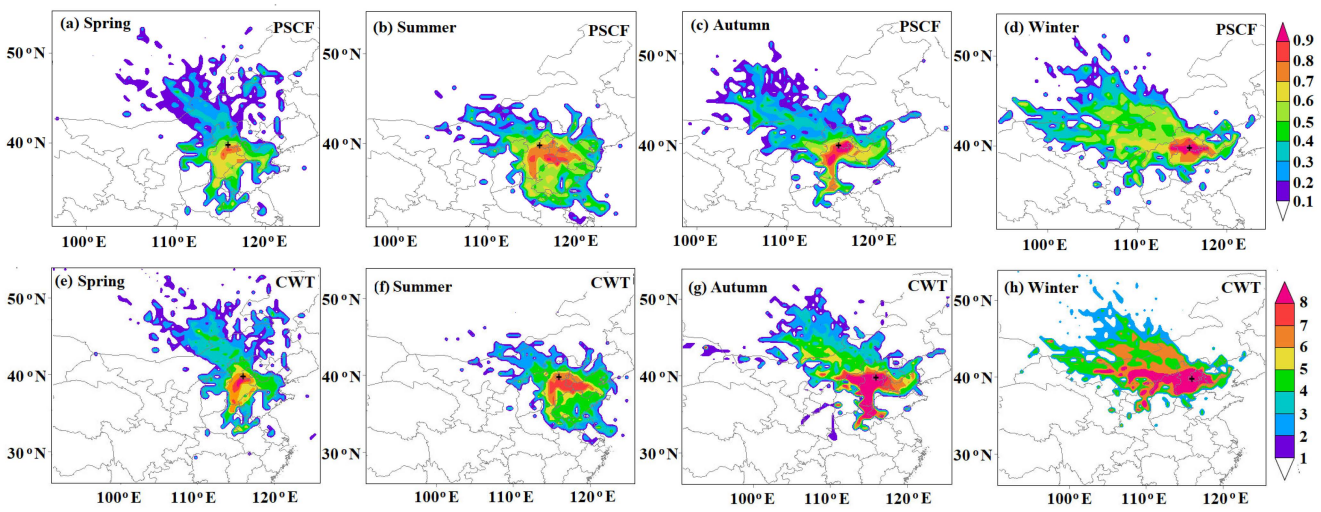

Figure 7. Seasonal PSCF (**a**–**d**) and CWT (**e**–**h**) maps for BC in Beijing in 2020. The cross denotes the studied city, and the values are displayed in color.

In autumn, Beijing was mainly affected by the air mass pathways in three directions: one from Mongolia and Inner Mongolia, another one from the Bohai Sea, and the third one

from southern Hebei. The air mass derived from Inner Mongolia traveled across northwestern Hebei and dispersed BC in Beijing (PSCF < 0.4 and CWT < 5 μg/m^3). Substantial contributions occurred in Tianjin, as well as the Bohai Sea, with PSCF and CWT values exceeding 0.6 and 6 μg/m^3. On the contrary, southern Hebei was the most noteworthy potential source area, with high PSCF and CWT values contributing up to 0.8 and 8 μg/m^3, respectively. The agriculture is well developed in Hebei, resulting in the large amounts of BC originating from the biomass burning processes during harvesting season. The correspondingly short air mass backward trajectories represent that air mass moves slowly, which leads to BC accumulation. BC pollution was noticed to be more striking for winter (10.68 μg/m^3) than autumn (8.39 μg/m^3) in Beijing. The PSCF and CWT results indicated that most regions of Hebei, Tianjin, and northern Shanxi were the main potential source regions with PSCF > 0.6 and CWT > 7 μg/m^3. The air mass originated in central Inner Mongolia and northern Shanxi, passing through Hebei from west to east and mixing with local emissions from Beijing, which tended to cause large-scale BC pollution under adverse weather conditions. In addition to local emissions, cross-boundary transport was also crucial to BC pollution. The central region of Hebei Province around Beijing has adversely affected the BC of Beijing (PSCF: 0.6–0.9, and CWT: 6–8 μg/m^3).

Located at the east end of YRD, Shanghai is the economic center of China. Figure 8 portrays that the potential sources differed in four seasons for Shanghai. High PSCF/CWT to BC values were noticed mainly over the western regions of Shanghai in spring, including southern Jiangsu and northern Zhejiang province, with a PSCF > 0.8 and CWT > 3 μg/m^3. The Jiaodong Peninsula, northern Jiangsu, and eastern Anhui also distributed high PSCF with ~0.6 and ordinary CWT with ~2 μg/m^3. During summer, air masses primarily come from relatively clean areas under the prevailing southeast wind, while air masses derived from the ocean can carry abundant water vapor and further form precipitation. Suzhou in Jiangsu province and Jiaxing and Shaoxing in Zhejiang province were identified as principal potential source areas of BC by PSCF/CWT models (PSCF > 0.7 and CWT near 3 μg/m^3). The autumn-time PSCF/CWT display high values in the South Jiangsu Province (0.7–0.9 for PSCF, 3–5 μg/m^3 for CWT), which demonstrated a large BC contribution from the surrounding cities, such as Suzhou, Wuxi, and Nanjing. The potential pollution source of BC with long-range transport was also observed in Chuzhou, Bengfu, Huainan, and Heifei of Northwest Anhui Province. In cold winter, the major BC potential source was found to be distinguished from those in the other three seasons, with high PSCF/CWT peaks covering most of the YRD region, especially in Jiaxing, Suzhou, Wuxi, Nantong, Taizhou, and Changzhou, revealing a regional BC pollution in the wintertime. Meanwhile, considering the prevailing northerly wind in winter, a wider-ranging distribution of PSCF and CWT was identified. Shanghai has a weak contribution to BC from distant North Heibei, Shandong Province, and Tianjin, with PSCF basically between 0.5 and 0.7 and CWT between 2 and 4 μg/m^3. Additionally, The Yellow Sea and the East China Sea were also potential sources of BC (PSCF > 0.4 and CWT > 2 μg/m^3).

Guangzhou, the capital of Guangdong Province, is situated at the center of PRD. Figure 9 illustrates the spatial distribution of PSCF and CWT in Guangzhou in 2020. In spring, the major potential sources for BC with high PSCF (>0.7) and slightly high CWT (1.8–2.1 μg/m^3) were located at the northeast terrestrial side of Guangzhou, comprising cities of Qingyuan, Shaoguan, Huizhou, Dongguang, Shanwei, Heyuan in North Guangdong province, Ganzhou and Ji'an in south Jiangxi province. Clean airflow from the South China Sea promoted extremely low BC concentrations in Guangzhou during summer. Compared to the range of potential source regions in spring, the scope in hot summer rapidly shrank, only covering part of Guangdong province and the South China Sea. The CWT values were fairly lower in Guangzhou, with the value below 2.1 μg/m^3 in spring, summer, and autumn, whilst winter increases (<3.3 μg/m^3) are not so obvious as in Beijing and Shanghai due to less residential heating needs in winter. The PSCF/CWT values in winter had similar distributions to those of spring, with more centralized values located at the Jieyang, Shanwei, and Huizhou with a PSCF > 0.8 and CWT ~3 μg/m^3. Particularly,

the East China Sea, South China Sea, and the adjacent coastal region were also identified as potential sources of BC region (PSCF: 0.2–0.8, and CWT: 0.6–2.7 μg/m^3), probably due to the heavy oil combustion as the busy commercial shipping in the coastal water.

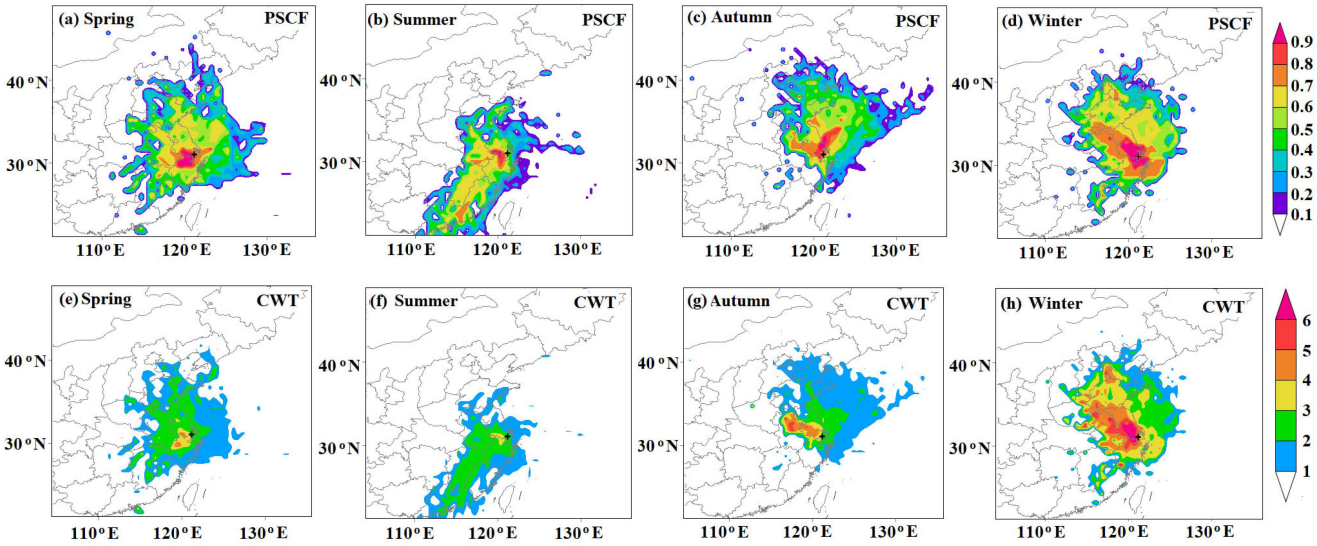

Figure 8. Seasonal PSCF (**a**–**d**) and CWT (**e**–**h**) in Shanghai in 2020. The cross denotes the studied city, and the values are displayed in color.

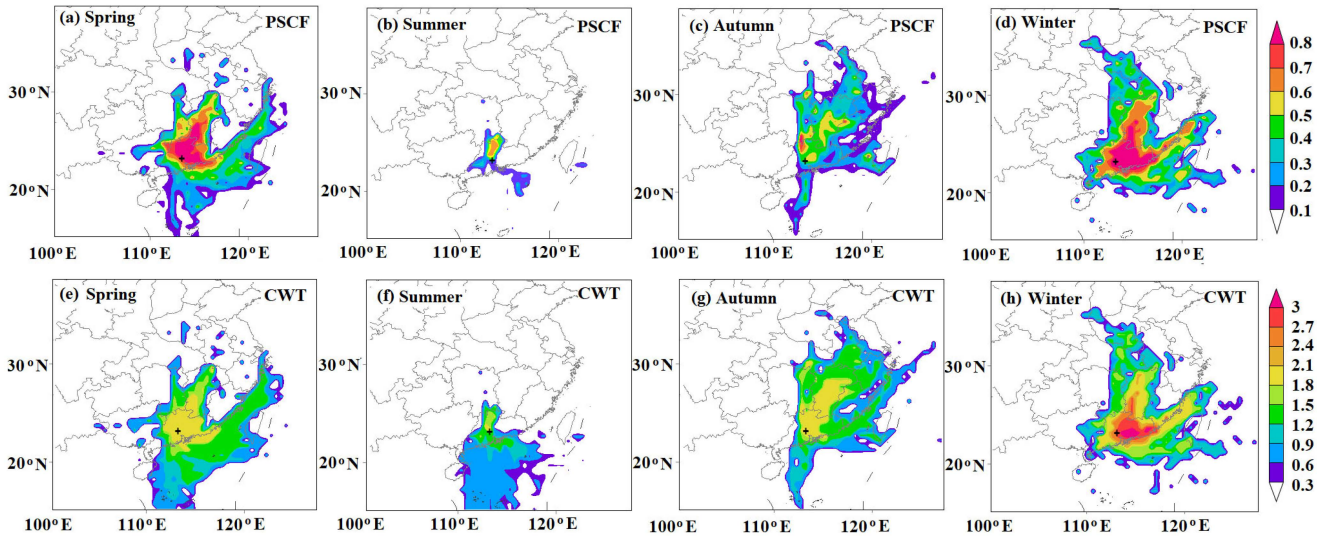

Figure 9. Seasonal PSCF (**a**–**d**) and CWT (**e**–**h**) maps for BC in Guangzhou in 2020. The cross denotes the studied city, and the values are displayed in color.

Chengdu, the capital of Sichuan province, is located in the west of the SB and the eastern edge of the Qinghai-Tibetan plateau. On any given season, the east, northeast, and southeast winds from the mid-east of the SB are significantly more frequent in Chengdu due to its distinctive geographical pattern. Accordingly, BC concentrations are affected by regional transport under the domination of prejudiced east winds. The results of PSCF and CWT in Chengdu in 2020 are displayed in Figure 10. In spring, the potential source region was concentrated in Chengdu and adjacent cities, with PSCF values of 0.6–0.7 and CWT of ~5 μg/m^3. Hanzhong in the south Shaanxi province was also a non-negligible source region of BC in spring associated with the long-range transport (PSCF: 0.4–0.6, and CWT: 4–5 μg/m^3). The average BC level during summer (4.62 μg/m^3) is slightly lower than that in spring (4.76 μg/m^3). The potential source region of high PSCF and CWT

values mildly narrowed in summer, whilst high contribution in SB was mostly centralized in Luzhou, Zigong, Suining, and southwest Chongqing with PSCF of 0.6 and CWT of 5 μg/m^3. In autumn, the most potential source region of BC was located in the southeast of SB, covering Meishan, Zigong, Neijing, Ziyang, Suining, and Deyang in Sichuan province, eastern Chongqing, and Zunyi in Guizhou province with PSCF > 0.8 and CWT > 7 μg/m^3. Some coal and chemical-related industries are situated in the region, which is recognized as an important area for producing BC. The other source region with large amounts of BC (PSCF > 0.7 and CWT > 5 μg/m^3) was located at the northeastern Mianyang, Guangyuan, Nanchong, Bazhong, and Dazhou. In winter, high PSCF (>0.8) and CWT (>7 μg/m^3) peak, located in the east and southeast of Chengdu in autumn, spread to most areas of SB, indicative of severe regional BC pollution within the basin under control of the local weather with low wind speeds and weak air circulation. The trails of long-range transport from north and west were relatively inferior.

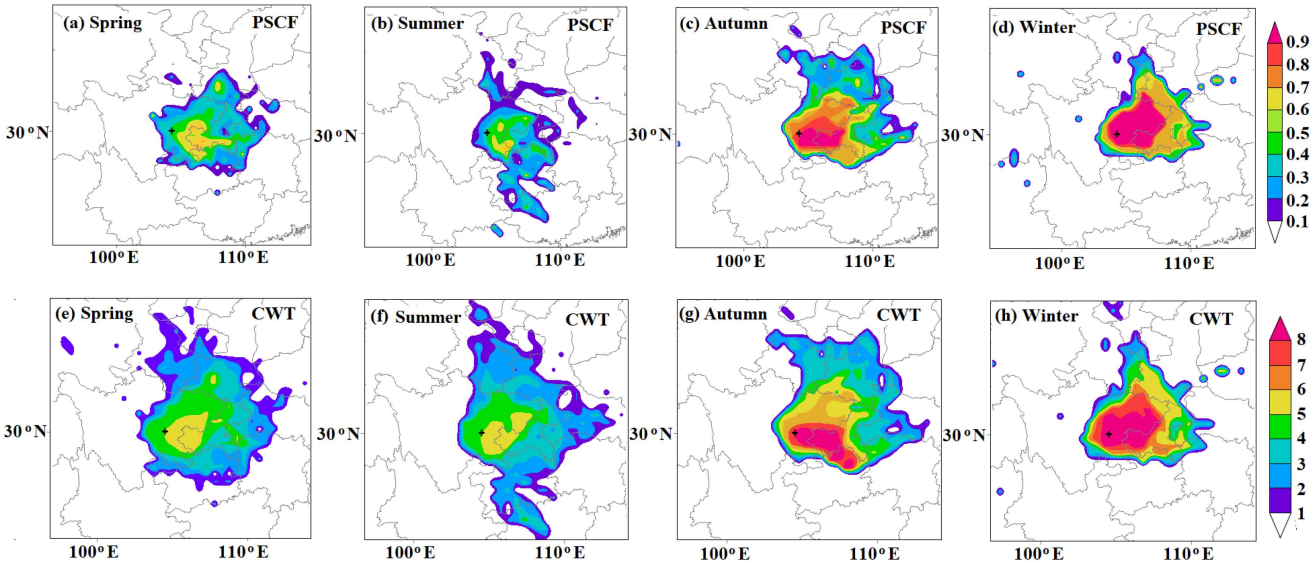

Figure 10. Seasonal PSCF (**a**–**d**) and CWT (**e**–**h**) maps for BC in Chengdu in 2020. The cross denotes the studied city, and the values are displayed in color.

Generally, most potential source areas with high PSCF/CWT values for BC were located in the surroundings of the studied city, and local sources made a major contribution to BC. BC emitted in other, particularly remote areas, are largely dispersed in the air. This is confirmed during days with smog occurrence when the weather is breezy, and it is primarily local emission sources that are associated with the concentration of pollutants. Compared to Shanghai and Guangzhou, Beijing and Chengdu are more BC-polluted areas. Beijing is located in the BTH, and the long-distance regional transport contributes significantly to BC pollution in Beijing. The geographical location of Chengdu leads to the transport and accumulation of BC inside the basin, and the potential source region is mainly concentrated in the territory of Sichuan province and nearby Chongqing.

4. Conclusions

The detailed characteristics of atmospheric MERRA-2 BC over China from 1981 to 2020 are investigated based on the MERRA-2 reanalysis dataset. The MERRA-2 surface concentrations generally portray a good correlation with ground-based measurements around China, with the highest accuracy in the Northwest (R = 0.91) and lowest in the Southwest and Northeast (R = 0.57). The spatial, annual, seasonal, and monthly variations of BC concentration and its estimated potential source region over China, including representative regions, are systematically investigated. In recent 40 years, the annual-averaged MERRA-2 BC presents diverse spatial distributions over China with an average value

of 1.15 μg/m^3, and it shows a fast growth rate during 1981–2007 and a relatively slow decrease after that. The monthly mean BC concentrations vary almost 2 fold, ranging from the lowest 0.89 μg/m^3 in July to the highest 1.50 μg/m^3 in December. The winter season has the highest mean concentration of BC, followed by autumn and spring, whereas summer shows relatively weaker values.

The annual average BC concentrations during 1981–2020 follow the order of BTH (4.02 μg/m^3) > SB (3.94 μg/m^3) > YRD (2.68 μg/m^3) > PRD (1.47 μg/m^3). The monthly average BC concentration in BTH, YRD, PRD, and SB regions portray the smallest 3.18 μg/m^3 in May, 1.94 μg/m^3 in August, 0.82 μg/m^3 in July, 3.04 μg/m^3 in June, respectively, whereas the peak events of BC occur consistently in December, and the average BC concentrations for BHT, YRD, PRD, and SB are 5.09 μg/m^3, 3.83 μg/m^3, 2.12 μg/m^3, and 5.41 μg/m^3, respectively. The most potential source areas for BC are concentrated in the local and surrounding areas of the research city. Compared to Shanghai and Guangzhou, Beijing and Chengdu are more BC-polluted areas. Beijing is located in the BTH, and the long-distance regional transport contributes significantly to BC pollution in Beijing, especially under the influence of prevailing southerly winds. The geographical location of Chengdu causes the transfer and accumulation of BC inside SB. Taking into account the high BC levels, further legislation efforts are expected to suppress pollution and improve air quality in these areas.

Supplementary Materials: The following supporting information can be downloaded at: https://www.mdpi.com/article/10.3390/atmos14091378/s1, Figure S1: Comparison of the monthly average MERRA-2 BC concentration and ground observations over China. Table S1: Information of the ground-based sites over China.

Author Contributions: Conceptualization, M.M. and X.Z.; methodology, M.M.; software, Y.Z.; validation, Y.Z. and M.M.; formal analysis, M.M.; investigation, Y.Z.; resources, Y.Z.; data curation, M.M. and X.Z.; writing—original draft preparation, M.M.; writing—review and editing, M.M.; visualization, X.Z.; supervision, X.Z.; project administration, M.M.; funding acquisition, M.M. All authors have read and agreed to the published version of the manuscript.

Funding: This work is financially supported by the Qinglan Project, the State Key Laboratory of Atmospheric Boundary Layer Physics and Atmospheric Chemistry (LAPC-KF-2023-09).

Institutional Review Board Statement: Not applicable.

Informed Consent Statement: Not applicable.

Data Availability Statement: The data is available upon request.

Acknowledgments: Analyses and visualizations used in this paper were produced with the Giovanni online data system developed and maintained by the NASA GES DISC. We also acknowledge the mission scientists and Principal Investigators who provided the data used in this research effort.

Conflicts of Interest: The authors declare no conflict of interest.

References

1. Bond, T.C.; Streets, D.G.; Yarber, K.F.; Nelson, S.M.; Woo, J.H.; Klimont, Z. A technology-based global inventory of black and organic carbon emissions from combustion. *J. Geophys. Res.* **2004**, *109*, D14203. [CrossRef]
2. Jia, H.H.; Pan, J.; Huo, J.T.; Fu, Q.Y.; Duan, Y.S.; Lin, Y.F.; Hu, X.; Cheng, J.P. Atmospheric black carbon in urban and traffic areas in Shanghai: Temporal variations, source characteristics, and population exposure. *Environ. Pollut.* **2021**, *289*, 117868. [CrossRef]
3. Koch, D.; Del Genio, A.D. Black carbon semi-direct effects on cloud cover: Review and synthesis. *Atmos. Chem. Phys.* **2010**, *10*, 7685–7696. [CrossRef]
4. Guo, B.; Wang, Y.Q.; Zhang, X.Y.; Che, H.Z.; Ming, J.; Yi, Z.W. Long-term variation of black carbon aerosol in China based on revised aethalometer monitoring data. *Atmosphere* **2020**, *11*, 684. [CrossRef]
5. Bond, T.C.; Doherty, S.J.; Fahey, D.W.; Forster, P.M.; Berntsen, T.; DeAngelo, B.J.; Flanner, M.G.; Ghan, S.; Kaercher, B.; Koch, D.; et al. Bounding the role of black carbon in the climate system: A scientific assessment. *J. Geophys. Res.* **2013**, *118*, 5380–5552. [CrossRef]
6. Menon, S.; Hansen, J.; Nazarenko, L.; Luo, Y.F. Climate effects of black carbon aerosols in China and India. *Science* **2002**, *297*, 2250–2253. [CrossRef]
7. Ramanathan, V.; Carmichael, G. Global and regional climate changes due to black carbon. *Nat. Geosci.* **2008**, *1*, 221–227. [CrossRef]

8. Verma, S.; Pani, S.K.; Bhanja, S.N. Sources and radiative effects of wintertime black carbon aerosols in an urban atmosphere in east India. *Chemosphere* **2013**, *90*, 260–269. [CrossRef] [PubMed]
9. Guilloteau, A.; Bedjanian, Y.; Nguyen, M.L.; Tomas, A. Desorption of polycyclic aromatic hydrocarbons from a soot surface: Three- to fifive-ring PAHs. *J. Phys. Chem. A* **2009**, *114*, 942–948. [CrossRef] [PubMed]
10. Barrado, A.I.; Garcia, S.; Sevillano, M.L.; Rodriguez, J.A.; Barrado, E. Vaporphase concentrations of PAHs and their derivatives determined in a large city: Correlations with their atmospheric aerosol concentrations. *Chemosphere* **2013**, *93*, 1678–1684. [CrossRef]
11. Pani, S.K.; Wang, S.H.; Lin, N.H.; Chantara, S.; Lee, C.T.; Thepnuan, D. Black carbon over an urban atmosphere in northern peninsular Southeast Asia: Characteristics, source apportionment, and associated health risks. *Environ. Pollut.* **2020**, *259*, 113871. [CrossRef]
12. Jia, L.; Cheng, P.; Yu, Y.; Chen, S.H.; Wang, C.X.; He, L.; Nie, H.T.; Wang, J.C.; Zhang, J.C.; Fan, B.G.; et al. Regeneration mechanism of a novel high performance biochar mercury adsorbent directionally modified by multimetal multilayer loading. *J. Environ. Manag.* **2023**, *326*, 116790. [CrossRef]
13. Shrestha, G.; Traina, S.J.; Swanston, C.W. Black carbon's properties and role in the environment: A comprehensive review. *Sustainability* **2010**, *2*, 294–320. [CrossRef]
14. Zhao, X.S.; Wan, Z.; Zhu, H.G.; Chen, R.P. The carcinogenic potential of extractable organic matter from urban airborne particles in Shanghai China. *Mutat. Res. Genet. Toxicol. Environ. Mutagen.* **2003**, *540*, 107–117. [CrossRef]
15. Li, L.Y.; Hu, D.Y.; Zhang, W.L.; Cui, L.Y.; Jia, X.; Yang, D.; Liu, S.; Deng, F.R.; Liu, J.X.; Guo, X.B. Effect of short-term exposure to particulate air pollution on heart rate variability in normal-weight and obese adults. *Environ. Health* **2021**, *20*, 29. [CrossRef]
16. Rabito, F.A.; Yang, Q.; Zhang, H.; Werthmann, D.; Shankar, A.; Chillrud, S. The association between short-term residential black carbon concentration on blood pressure in a general population sample. *Indoor Air* **2020**, *30*, 767–775. [CrossRef]
17. Hoek, G.; Boogaard, H.; Knol, A.; De Hartog, J.; Slottje, P.; Ayres, J.G.; Borm, P.; Brunekreef, B.; Donaldson, K.; Forastiere, F.; et al. Concentration response functions for ultrafifine particles and all-cause mortality and hospital admissions: Results of a European expert panel elicitation. *Environ. Sci. Technol.* **2010**, *44*, 476–482. [CrossRef]
18. Wang, Y.Y.; Li, X.; Shi, Z.H.; Huang, L.; Li, J.Y.; Zhang, H.L.; Ying, Q.; Wang, M.; Ding, D.P.; Zhang, X.L.; et al. Premature mortality associated with exposure to outdoor black carbon and its source contributions in China. *Resour. Conserv. Recycl.* **2021**, *170*, 105620. [CrossRef]
19. Farzad, K.; Khorsandi, B.; Khorsandi, M.; Bouamra, O.; Maknoon, R. A study of cardiorespiratory related mortality as a result of exposure to black carbon. *Sci. Total Environ.* **2020**, *725*, 138422. [CrossRef]
20. Surya, S.R.; Rahiman, M.A. Cloud Detection from Satellite Images Based on Haar Wavelet and Clustering. In Proceedings of the International Conference on Nextgen Electronic Technologies, Silicon to Software (Icnets2), Chennai, India, 23–25 March 2017; pp. 163–167.
21. Mousivand, A.; Verhoef, W.; Menenti, M.; Gorte, B. Modeling top of atmosphere radiance over heterogeneous non-lambertian rugged terrain. *Remote Sens.* **2015**, *7*, 8019–8044. [CrossRef]
22. Bengtsson, L.; Shukla, J. Integration of space and in situ observations to study global climate change. *Bull. Am. Meteorol. Soc.* **1988**, *69*, 1130–1143. [CrossRef]
23. Wang, W.; Xie, P.; Yoo, S.-H.; Xue, Y.; Kumar, A.; Wu, X. An assessment of the surface climate in the NCEP climate forecast system reanalysis. *Clim. Dyn.* **2011**, *37*, 1601–1620. [CrossRef]
24. Ukhov, A.; Mostamandi, S.; Da Silva, A.; Flemming, J.; Alshehri, Y.; Shevchenko, I.; Stenchikov, G. Assessment of natural and anthropogenic aerosol air pollution in the Middle East using MERRA-2, CAMS data assimilation products, and highresolution WRF-Chem model simulations. *Atmos. Chem. Phys.* **2020**, *20*, 9281–9310. [CrossRef]
25. Qin, W.H.; Zhang, Y.P.; Chen, J.; Yu, Q.; Cheng, S.M.; Li, W.G.; Liu, X.A.; Tian, H.Z. Variation, sources and historical trend of black carbon in Beijing, China based on ground observation and MERRA-2 reanalysis data. *Environ. Pollut.* **2019**, *245*, 853–863. [CrossRef]
26. Pfenninger, S.; Staffell, I. Long-term patterns of European PV output using 30 years of validated hourly reanalysis and satellite data. *Energy* **2016**, *114*, 1251–1265. [CrossRef]
27. Wang, R.; Tao, S.; Wang, W.; Liu, J.; Shen, H.; Shen, G.; Wang, B.; Liu, X.; Li, W.; Huang, Y.; et al. Black carbon emissions in China from 1949 to 2050. *Environ. Sci. Technol.* **2012**, *46*, 7595–7603. [CrossRef]
28. Mao, Y.H.; Liao, H.; Han, Y. Impacts of meteorological parameters and emissions on decadal and interannual variations of black carbon in China for 1980–2010. *J. Geophys. Res. Atmos.* **2016**, *121*, 1822–1843. [CrossRef]
29. Sasser, E.; Hemby, J.; Adler, K.; Anenberg, S.; Bailey, C.; Brockman, L.; Frank, N. *Report to Congress on Black Carbon*; Department of the Interior Environment and Related Agencies: Washington, DC, USA, 2012.
30. Wilkening, K.E.; Barrie, L.A.; Engle, M. Trans-pacific air pollution. *Science* **2000**, *290*, 65–67. [CrossRef]
31. Cao, S.S.; Zhang, S.Q.; Cao, C.C.; Yan, Y.Y.; Bao, J.H.; Su, L.; Liu, M.Q.; Peng, N.; Liu, M. A long-term analysis of atmospheric black carbon MERRA-2 concentration over China during 1980–2019. *Atmos. Environ.* **2021**, *264*, 118662. [CrossRef]
32. Xu, X.F.; Yang, X.Y.; Zhu, B.; Tang, Z.W.; Wu, H.; Xie, L.F. Characteristics of MERRA-2 back carbon variation is east China during 2000–2016. *Atmos. Environ.* **2020**, *222*, 117140. [CrossRef]
33. Zhao, J.W.; Liu, Y.X.; Shan, M.; Liang, S.; Cui, C.; Chen, L.; Cao, S.; Mao, J.; Zhan, H.; Sun, Y.L.; et al. Characteristics, potential regional sources and health risk of black carbon based on ground observation and MERRA-2 reanalysis data in a coastal city, China. *Atmos. Res.* **2021**, *256*, 105563. [CrossRef]

34. Randles, C.A.; da Silva, A.M.; Buchard, V.; Colarco, P.R.; Darmenov, A.; Govindaraju, R.; Smirnov, A.; Holben, B.; Ferrare, R.; Hair, J.; et al. The MERRA-2 aerosol reanalysis, 1980 onward. Part I: System description and data assimilation evaluation. *J. Clim.* **2017**, *30*, 6823–6850. [CrossRef]
35. Buchard, V.; Randles, C.A.; da Silva, A.M.; Darmenov, A.; Colarco, P.R.; Govindaraju, R.; Ferrare, R.; Hair, J.; Beyersdorf, A.J.; Ziemba, L.D.; et al. The MERRA-2 aerosol reanalysis, 1980 onward. Part II: Evaluation and case studies. *J. Clim.* **2017**, *30*, 6851–6872. [CrossRef] [PubMed]
36. Gelaro, R.; McCarty, W.; Suárez, M.J.; Todling, R.; Molod, A.; Takacs, L.; Randles, C.A.; Darmenov, A.; Bosilovich, M.G.; Reichle, R.; et al. The Modern-Era retrospective analysis for research and applications, version 2 (MERRA-2). *J. Clim.* **2017**, *30*, 5419–5454. [CrossRef]
37. The Goddard Earth Sciences (GES) Data and Information Services Center (DISC). Available online: https://disc.gsfc.nasa.gov (accessed on 30 July 2023).
38. Ashbaugh, L.L.; Malm, W.C.; Sadeh, W.Z. A residence time probability analysis of sulfur concentrations at Grand Canyon National Park. *Atmos. Environ.* **1985**, *19*, 1263–1270. [CrossRef]
39. The Global Data Assimilation System (GDAS). Available online: https://www.ncei.noaa.gov/access/metadata/landing-page/bin/iso?id=gov.noaa.ncdc:C00379 (accessed on 30 July 2023).
40. Polissar, A.V.; Hopke, P.K.; Poirot, R.L. Atmospheric aerosol over Vermont: Chemical composition and sources. *Environ. Sci. Technol.* **2001**, *35*, 4604–4621. [CrossRef]
41. Dimitriou, K.; Kassomenos, P. Three year study of tropospheric ozone with back trajectories at a metropolitan and a medium scale urban area in Greece. *Sci. Total Environ.* **2015**, *502*, 493–501. [CrossRef] [PubMed]
42. Hsu, Y.K.; Holsen, T.M.; Hopke, P.K. Comparison of hybrid receptor models to locate PCB sources in Chicago. *Atmos. Environ.* **2003**, *37*, 545–562. [CrossRef]
43. Mao, M.; Zhang, X.; Shao, Y.; Yin, Y. Spatiotemporal Variations and Factors of Air Quality in Urban Central China during 2013–2018. *Int. J. Environ. Res. Public Health* **2020**, *17*, 229. [CrossRef] [PubMed]
44. Liu, B.; Wu, J.; Zhang, J.; Wang, L.; Yang, J.; Liang, D.; Dai, Q.; Bi, X.; Feng, Y.; Zhang, Y.; et al. Characterization and source apportionment of PM2.5 based on error estimation from EPA PMF 5.0 model at a medium city in China. *Environ. Pollut.* **2017**, *222*, 10–22. [CrossRef]
45. Zheng, H.; Kong, S.F.; Yan, Q.; Wu, F.Q.; Cheng, Y.; Zheng, S.R.; Wu, J.; Yang, G.W.; Zheng, M.M.; Tang, L.; et al. The impacts of pollution control measures on PM2.5 reduction: Insights of chemical composition, source variation and health risk. *Atmos. Environ.* **2019**, *197*, 103–117. [CrossRef]
46. Wang, W.F.; Yu, J.; Cui, Y.; He, J.; Xue, P.; Cao, W.; Ying, H.M.; Cao, W.K.; Yan, Y.C.; Hu, B.; et al. Characteristics of fifine particulate matter and its sources in an industrialized coastal city, Ningbo, Yangtze River Delta, China. *Atmos. Res.* **2018**, *203*, 105–117. [CrossRef]
47. Mao, M.; Rao, L.; Jiang, H.; He, S.; Zhang, X. Air Pollutants in Metropolises of Eastern Coastal China. *Int. J. Environ. Res. Public Health* **2022**, *19*, 15332. [CrossRef] [PubMed]
48. Luo, Y.X.; Chen, J.; Zheng, X.B. Climatology of aerosol optical depth over China from recent 10 years of MODIS remote sensing data. *Ecol. Environ. Sci.* **2012**, *21*, 876–883. [CrossRef]
49. *GB 3095-2012*; Ambient Air Quality Standards. Ministry of Environmental Protection of PRC: Beijing, China, 2012.
50. Shen, L.J.; Wang, H.L.; Kong, X.C. Characterization of black carbon aerosol in the Yangtze River Delta, China: Seasonal variation and source apportionment. *Atmos. Pollut. Res.* **2021**, *12*, 195–209. [CrossRef]
51. Zhao, Q.Y.; Zhao, W.; Bi, J. Climatology and calibration of MERRA-2 PM2.5 components over China. *Atmos. Pollut. Res.* **2021**, *12*, 357–366. [CrossRef]
52. Mao, M.; Zhang, X.; Yin, Y. Particulate matter and gaseous pollutions in three metropolises along the Chinese Yangtze River: Situation and Implications. *Int. J. Environ. Res. Public Health* **2018**, *15*, 1102. [CrossRef]
53. Ye, W.F.; Ma, Z.Y.; Ha, X.Z. Spatial-temporal patterns of PM2.5 concentrations for Chinese cities. *Sci. Total Environ.* **2018**, *631–632*, 524–533. [CrossRef]
54. Zhang, Z.S.; Gao, J.; Engling, G.; Tao, J.; Chai, F.; Zhang, L.; Zhang, R.; Sang, X.; Chan, C.Y.; Lin, Z.; et al. Characteristics and applications of size-segregated biomass burning tracers in China's Pearl River Delta region. *Atmos. Environ.* **2015**, *102*, 290–301. [CrossRef]
55. Zhang, Y.L.; Cao, F. Is it time to tackle PM2.5 air pollutions in China from biomass-burning emissions. *Environ. Pollut.* **2015**, *202*, 217–219. [CrossRef]